Plasma activation and its nanoconfinement effects boost surface anti-biofouling performance

Mahmoodi, Nasim; Bazzoli, Dario; Overton, Tim; Mendes, Paula

DOI:
10.1002/admi.202202087

Document Version
Publisher's PDF, also known as Version of record

Citation for published version (Harvard):
Mahmoodi, N, Bazzoli, D, Overton, T & Mendes, P 2023, 'Plasma activation and its nanoconfinement effects boost surface anti-biofouling performance', *Advanced Materials Interfaces*, vol. 10, no. 6, 2202087. https://doi.org/10.1002/admi.202202087

ADVANCED MATERIALS INTERFACES
www.advmatinterfaces.de

Plasma Activation and its Nanoconfinement Effects Boost Surface Anti-Biofouling Performance

Nasim Mahmoodi, Dario G. Bazzoli, Tim W. Overton, and Paula M. Mendes**

Although plasma treatment can alter polymer surface wettability and adhesiveness, scant attention has been given to plasma effects across scales and their anti-fouling performance. Herein, the discovery that plasma-activated polydimethylsiloxane (PDMS) nanopillar arrays remarkably enhance anti-fouling behavior, yielding a 98.7% reduction in *Escherichia coli* adhesion compared to native planar surfaces. The plasma-activated nanopillar arrays can hold to their anti-fouling properties for extended periods of storage, still exhibiting more than 65.1% less bacterial colonization than their native planar counterparts after 50 days. The anti-fouling behavior promoted by plasma activation is significantly enhanced as the structure features reduce in size from macroscale to microscale to nanoscale, revealing an altered plasma activation effect upon confinement at the nanoscale level. It is anticipated that the findings will improve the ability to achieve non-fouling effects in polymeric materials for a broad range of applications in clinical and industrial settings.

1. Introduction

Bacterial attachment to material surfaces poses a major clinical and industrial problem as it is the first step of biofilm formation.[1–4] The physical and chemical properties of the material surface affect the interaction between the bacteria and the surface. The effect of physicochemical properties of the material such as surface charge density,[5,6] stiffness,[7] hardness,[8–10] surface roughness,[11,12] topography,[13,14] chemical composition,[15] and hydrophobicity[16] on the adhesion of the bacteria has been studied extensively. These findings highlight the importance of chemical and topographic modifications of the surface for the prevention and mitigation of bacterial attachment.

In the past decade, applications of topographies[17–22] inspired by natural antifouling or bactericidal surfaces such as lotus leaves,[23] shark skin,[24] cicada wing,[25,26] gecko skin,[27] and dragonfly wing[28] have shown a promising strategy in the area of anti-microbial and anti-fouling materials. The use of some nanoscale topographies inspired by natural bactericidal surfaces was found to be lethal for the bacteria.[29,30] The mechanism is based on cell membrane damage or rupture due to physical contact with these nanoscale features. However, there are some concerns regarding the use of these surfaces, as the dead bacteria provide a nutritious platform for subsequent bacteria approaching (and potentially attaching to) the surface.[31] Micro/nano surface topographies have also been shown to decrease bacterial attachment and mitigate biofilm formation. It has been shown that the features' shape, size, and distribution affect microbial attachment.[32] The general findings reveal that by reducing the dimension of the topographies, the number of attached bacteria decreases.[32–34]

Polydimethylsiloxane (PDMS) is a bulk polymer consisting of repeated units of $-OSi(CH_3)_2O-$ and known as one of the most extensively used materials for biomedical devices such as catheters, contact lenses, medical adhesives, finger joint implants, and drug delivery systems owing to a number of advantages: ease of replication procedure, biocompatibility, nontoxicity, optical transparency, durability, and low fabrication cost.[35] A micro/nano surface with highly ordered features can be reproduced using PDMS through a replica molding technique.[36,37] In the past two decades, various research has been performed to investigate the effect of engineered patterns on bacterial adhesion to PDMS surfaces. The main findings highlight the dependence of adhesion on bacterial dimension and shape relative to the dimensions of the PDMS surface features and the gap size between them.[38] It has been shown that when the gap size or dimensions of the patterned features are smaller than the bacteria, the adhesion decreases due to the reduced surface area available for binding.[39,40] While these studies provide important insights into the design and development of antifouling surfaces, they also raise important questions about whether, or how, these structured surfaces can be further manipulated for optimal anti-biofouling performance.

By virtue of its simplicity and scalability, plasma-induced surface modification illustrates a potentially exploitable pathway

N. Mahmoodi, D. G. Bazzoli, T. W. Overton, P. M. Mendes
School of Chemical Engineering
University of Birmingham
Birmingham B15 2TT, UK
E-mail: t.w.overton@bham.ac.uk; p.m.mendes@bham.ac.uk

The ORCID identification number(s) for the author(s) of this article can be found under https://doi.org/10.1002/admi.202202087.

DOI: 10.1002/admi.202202087

to promote antifouling behavior on PDMS materials. Through PDMS surface plasma activation, different reactions can take place, including the generation of silanol groups (Si–OH) that can form strong intermolecular bonds or undergo condensation reactions to yield siloxane bonds (Si–O–Si).[41,42] These processes can change the surface properties significantly, even if some temporarily, but little is known about how plasma-activation affects bacterial adhesion, whether to planar surfaces or those structured at the micro or nanoscale.

With this in mind, in this work, we set out to create and plasma-activate PDMS-based materials with different structural properties to elucidate their impact on bacterial adhesion. Arrays of PDMS pillars with a height of 800 nm, diameters ranging from 0.5 to 2.5 µm, and spacing of 0.5 and 1 µm were generated using a replication molding technique. To enable direct comparisons, planar PDMS surfaces were also investigated. Low-power air plasma was used to activate the generated surfaces, which were subsequently evaluated for their capability to prevent bacterial adhesion using *Escherichia coli*, a Gram-negative bacterium that is responsible for catheter-associated urinary tract and orthopedic implant infections.[43,44]

2. Results and Discussion

Our initial experiments were focused on establishing how the plasma-activated planar PDMS interface characteristics (hydrophilicity and charge) influence bacterial adhesion. Hydrophilicity and surface charge are key parameters that affect bacterial attachment to surfaces.[45] The effect of plasma treatment and the change in the hydrophobicity of PDMS has been broadly studied.[41,46–49] In general, plasma treatment makes the PDMS surface more hydrophilic, and the PDMS hydrophobicity is known to recover partially or entirely over time. The timescale for the hydrophobicity recovery can vary from hours to weeks, being dependent on the time of plasma treatment, the thickness of the PDMS sample, and storage conditions (e.g., temperature and storage medium).[47,50–54]

Given the variability introduced by different experimental parameters, it was important to generate, plasma-activate, and store planar PDMS surfaces in well-defined conditions. The individual PDMS sample was placed in 35 mm Petri dishes and plasma-treated for 100 s at 18 W. The samples were then stored at 20 °C in the air at atmospheric pressure.

In order to evaluate the hydrophilicity of the activated PDMS surfaces over time, the surfaces were tested for their water contact angle, and the data are presented in **Figure 1**. As a control, native PDMS samples were also analyzed. Native PDMS showed hydrophobic properties with advancing and receding contact angles of 120.2° ± 1.2 and 81.9° ± 2.4. This result is in good agreement with the reported value range for native PDMS 109–122°.[49,51,52,55–57] Upon exposure to plasma, the hydrophobic methyl groups ($Si–CH_3$) are changed into hydrophilic silanol groups (Si–OH), leading to highly hydrophilic surfaces. Several research groups have investigated the surface compositions of the plasma-treated PDMS samples. The XPS data showed that the oxygen content of the plasma-treated PDMS samples increases at the expense of carbon content, and the ATR-FTIR measurements confirmed the presence of silanol

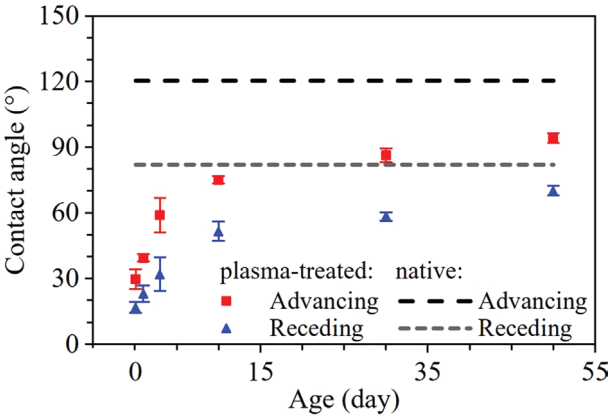

Figure 1. Hydrophobicity recovery of plasma-treated planar PDMS samples over 50 days; advancing and receding contact angles were measured for native and plasma-treated samples aged 2 h and 1, 3, 10, 30, and 50 days. The error bar represents SD.

groups in the treated samples.[47,51,58,59] For the samples with an age less than 2 h, the contact angle values were below 10°. The advancing contact angle for 2 h aged plasma-treated samples was 29.8° and increased gradually to 74.9° for 10 days aged samples, and thereafter minimal changes were observed for samples up to 50 days with the contact angle of 94.1°, which is the maximum time point in our study. It has been suggested that hydrophobicity recovery is due to the migration of free oligomers from the bulk to the surface and possibly a reorientation of the polar species into the bulk.[47,54,58] PDMS had not fully regained its initial hydrophobicity during this study time, and the advancing contact angle at saturation point was about 26.1° lower than native PDMS. The hydrophobicity recovery rate of the PDMS is slower than those obtained by Bodas et al. and Bacharouche et al.[42,60] The different behavior may be attributed to several factors, including the time of plasma treatment, the used plasma gas, the plasma power, and the storage conditions.

Previous studies highlighted the presence of negative surface charge on both native and oxidized PDMS samples.[61,62] However, in these studies, oxidized samples exhibited a more negative surface charge than native samples due to the presence of ionizable silanol groups on them.[63] The calorimetric method proposed by Uchida et al.[64] was used to investigate the effect of the age of plasma-treated planar PDMS on the surface charge. Toluidine Blue O (TBO) is a positively-charged dye[65] and was used to measure the surface charge for native and plasma-treated planar PDMS samples, which were aged 2 min and 1, 3, 10, 30, and 50 days. TBO makes a complex with the negative surface charge on the PDMS samples in a basic solution at pH 10, which can later be de-complexed in an aqueous acetic acid solution (50%, v/v). The surface charge of the treated samples was determined using the spectrophotometer absorbance readout of the decomplexation solution of TBO and expressed in terms of the mol of TBO per cm^2 using a calibration curve.

The ratio of TBO absorbance on the oxidized over native planar PDMS samples is plotted against the age of plasma-treated planar PDMS samples in **Figure 2**. TBO adsorption on native planar PDMS indicates the negative charge on the

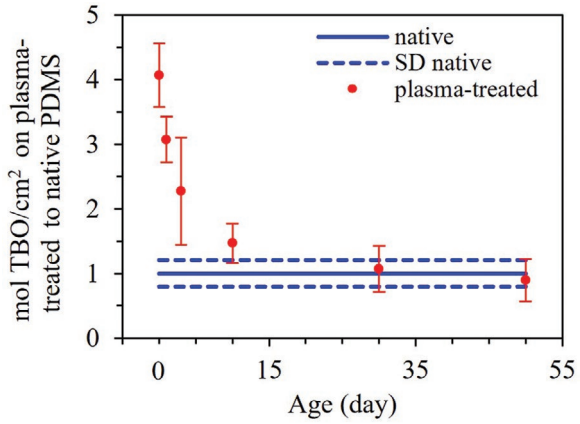

Figure 2. Relative surface charge of aged plasma-treated (aged 2 min and 1, 3, 10, 30, and 50 days) to native planar PDMS samples. The error bar represents SD.

surface. This result agrees with previously obtained negative zeta potential values on native planar PDMS that have been suggested to originate from the presence of impurities in the PDMS.[61,62,66–68] While native PDMS is characterized by a negatively charged surface, plasma treatment induced an increased negative charge density on the PDMS surface. For instance, the surface charge of the 2 min aged plasma-treated samples was 4-fold greater than the native sample. These results are in agreement with the formation of silanol groups on the PDMS surface, wherein a degree of deprotonation occurs in an aqueous solution, resulting in the presence of silanolate groups ($Si–O^-$) that renders the surface negatively charged.[63] The results showed a decrease in the surface charge with the age of the samples. However, the charge recovery is faster and more complete than hydrophilicity (Figure 1). The maximum negative charge was obtained for the 2 min aged sample and began to plateau after 10 days, in which it reached similar negative charge values as those of native PDMS samples. These findings are further evidence that reorganization of the PDMS polymer structure occurred over time with the migration of the polymer chains featuring Si–OH groups into the bulk.

Following the insights into the dependence of hydrophilicity and charge on the aging of the samples, these PDMS samples were used to investigate *E. coli* bacterial adhesion. *E. coli* SCC1 was selected to quantify the adhesion response on native (i.e., non-plasma-activated) planar and patterned PDMS samples. This strain expresses green fluorescent protein (GFP), making it easy for bacteria visualization.[69] The PDMS samples were incubated with *E. coli* suspension for 2 h at 30 °C in M63 minimal medium. Following incubation, the samples were washed to remove the loosely attached cells. Supainarez et al. showed that hydrodynamic forces due to the air/liquid interface can detach adherent bacteria from the surface.[70] To eliminate this effect, the samples were washed all the time in liquid without exposing the surface of the PDMS to air. This method of washing instead of dipping the PDMS a few times in fresh PBS[71] would avoid applying high shear stress due to the presence of air/liquid interface when removing the sample from the washing medium. After incubation, the Petri dish containing the PDMS sample was placed in a box filled with 500 ml of fresh PBS, which was then placed in a longitudinal shaker at 60 shakes per min for 90 s. This washing procedure has been performed twice with fresh PBS. The longitudinal movement applies shear force on the attached bacteria which leads to removing the loosely attached cells from the surface. Following the washing, the adhesion of bacteria on the PDMS surface was assessed by confocal microscopy and quantified in terms of the fraction of the covered area using ImageJ.

Figure 3A shows the ratio of the area coverage of *E. coli* on aged plasma-treated over native planar PDMS samples. The data were collected for native and plasma-treated planar samples aged 2 min, 2 h, and 1, 3, 10, 30, and 50 days. In general, plasma-treated PDMS samples have significantly better antifouling resistance compared to native PDMS. The results indicate that the bacterial adhesion on native PDMS is higher compared to the treated samples. A maximum reduction of 92–96% was observed for plasma-treated PDMS aged less than 1 day. The number of attached bacteria on the plasma-treated sample was significantly lower (p-value < 0.05) compared to the planar control native sample for all the aged samples, and the data suggests a positive correlation between the age of plasma-treated PDMS and bacterial coverage. After 50 days, the ratio is around 0.49, which represents a 51% reduction in the *E. coli* area coverage on plasma-treated compared to the native sample. Fluorescent microscopy reveals a regular arrangement of *E. coli* cells across the PDMS surface. Additional images are provided in Figure S1A, Supporting Information.

In order to better understand the role of the surface charge density of plasma-treated samples in the adhesion of *E. coli*, abiotic negatively charged carboxylic acid-modified polystyrene beads (PS-COOH, 1 µm diameter) were also evaluated for their adhesion to the PDMS surfaces. To be able to compare the adhesion behavior of the beads and *E. coli*, PS-COOH beads were suspended in M63 minimum medium to the optical density of 0.65 at 600 nm, which was the final optical density of *E. coli* after 2 h of incubation. After 2 h of incubation at 30 °C, the samples were washed. As shown in Figure 3B, the PS-COOH beads exhibited an adhesion profile similar to that of bacteria in the first few hours, with plasma-treated samples aged 2 min and 2 h exhibiting 85–90% reduction in bead adhesion over native PDMS samples (additional confocal microscopy images shown in Figure S1B, Supporting Information). These results strongly suggest that charge repulsion plays a key role in inhibiting *E. coli* adhesion to freshly plasma-treated PDMS samples, as the PDMS surface, PS-COOH beads, and *E. coli* all carry a negative charge.[72,73]

With longer aging times, the adhesion behavior for the beads and *E. coli* was found to be considerably different, with beads showing a higher adhesion to aged plasma-treated surfaces than native PDMS. For samples aged ≥ 10 days, the level of bead adhesion reached a plateau, with the aged samples displaying ≈4-fold more adhered beads than native PDMS surfaces. These results and the observed significant decrease in negative surface charge over aging time (Figure 2) indicate that electrostatic repulsion could no longer prevent adhesion between the anionic beads and aged samples, leading to the domination of other interfacial interactions. Since the beads interacted more favorably with the plasma-activated PDMS than native PDMS even after the samples have been aged for 50 days, it suggests

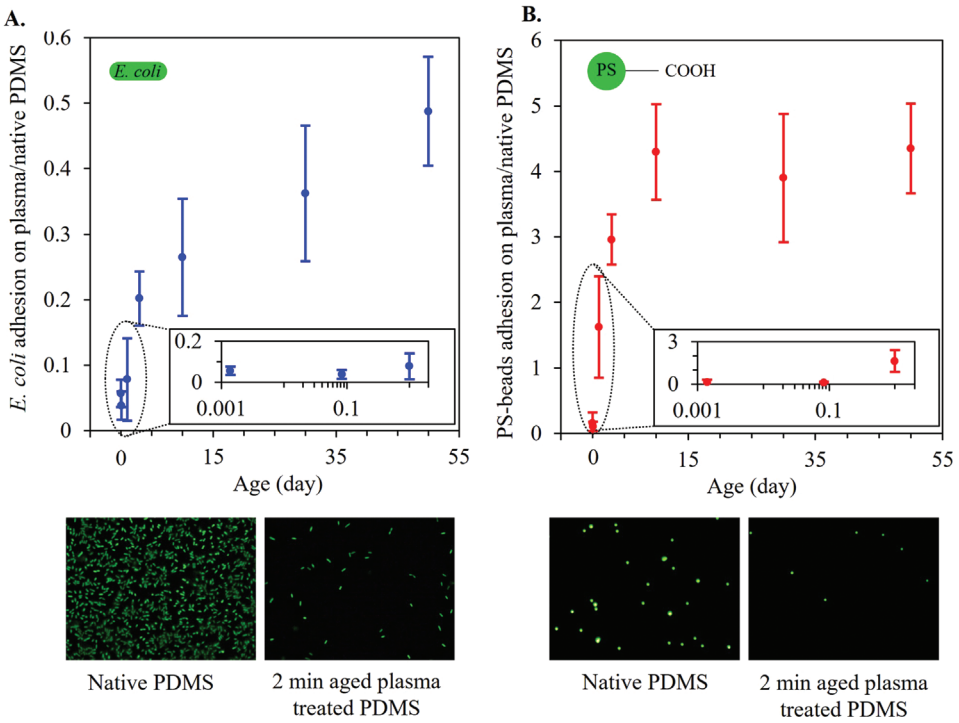

Figure 3. The ratio of the area coverage of A) *E. coli* SCC1 and B) PS beads for aged plasma-treated (samples aged 2 min, 2 h and 1, 3, 10, 30, and 50 days) over native planar PDMS. The error bar represents SD from three independent experiments.

that the plasma-activated PDMS surfaces have been altered with some long-lasting physicochemical characteristics. The enhanced adhesion of beads to plasma-treated surfaces can potentially be ascribed to multiple hydrogen bonding interactions between the carboxylic acid groups of the beads and the silanol groups on the activated PDMS.

The difference in adhesion trends between beads and *E. coli* also highlights that while surface charge prevents adhesion immediately after plasma treatment, hydrophilicity plays a more prominent role in aged samples. Notably, the increase in bacterial adhesion from aging of 10 days onwards follows a linear relationship (Figure 3A), with reduced adhesion even after 50 days of the aging time when compared with native samples. A similar linear relationship was observed for hydrophobicity recovery, in which the 50 days aged PDMS samples never recovered to the hydrophobicity observed in native samples.

The results from the planar plasma-activated PDMS samples revealed valuable insights into the relationship between their charge and hydrophilicity and their capability to inhibit bacterial adhesion. This knowledge sets the stage for the evaluation of bacterial adhesion on plasma-activated PMDS surfaces when they occur as micro or nanostructured surfaces.

Bacterial adhesion to structured surfaces is known to be affected by parameters such as the size, shape, and density of the surface features,[32,74] and thus these parameters were considered as factors that could act in concert with the changes in surface chemistry induced by plasma to control bacterial adhesion. PDMS micro and nanopillar arrays were fabricated with a height of 800 nm and diameters of 0.5, 1, and 2.5 µm and spacing of 0.5 and 1 µm. These structured surfaces cover feature dimensions that are equally sized, larger, or smaller than *E. coli*, which have an approximate shape of a spherocylinder of the length 2 µm and width 1 µm.[75]

The test specimen (160 × 40 mm) consists of six different patterns (0.5 × 0.5 mm), separated by a smooth planar area and arranged by two rows and three columns (**Figure 4**A). This setup is advantageous for two reasons. First, it allows the different surfaces to be exposed to the same bacterial culture conditions, removing batch effects from data. Second, analysis of the surfaces can be done simultaneously after the experiments. As part of the analysis, each individual patterned area had a corresponding planar area, with a maximum distance of 1 mm from each other to eliminate the effect of washing along the length of the test specimen and potential edge/central effects. Figure 4B represents the flow of the PDMS micro/nanopillar arrays replication from a silicon master mold. The scanning electron microscopy (SEM) micrographs of the fabricated pillars are presented in Figure 4C.

Bacterial adhesion experiments were conducted following similar incubation, washing, and analysis steps as described above for the planar surfaces. To start with, native (non-plasma-treated) structured surfaces were evaluated for their ability to affect bacterial adhesion. The ratio of bacterial coverage on native pillars to native planar area is shown in **Figure 5**. The coverage of *E. coli* on the different topological regions, except for D0.5S0.5, increased compared to the planar area (Figure S2A, Supporting Information). The highest coverage was observed for D1S1 with an average of 27% increase in adhesion compared to the planar control area. These results agree with previously reported data,[76,77] in which there is a dimensional threshold associated with the size of bacteria above which the topological features promote adhesion. The mechanism is suggested

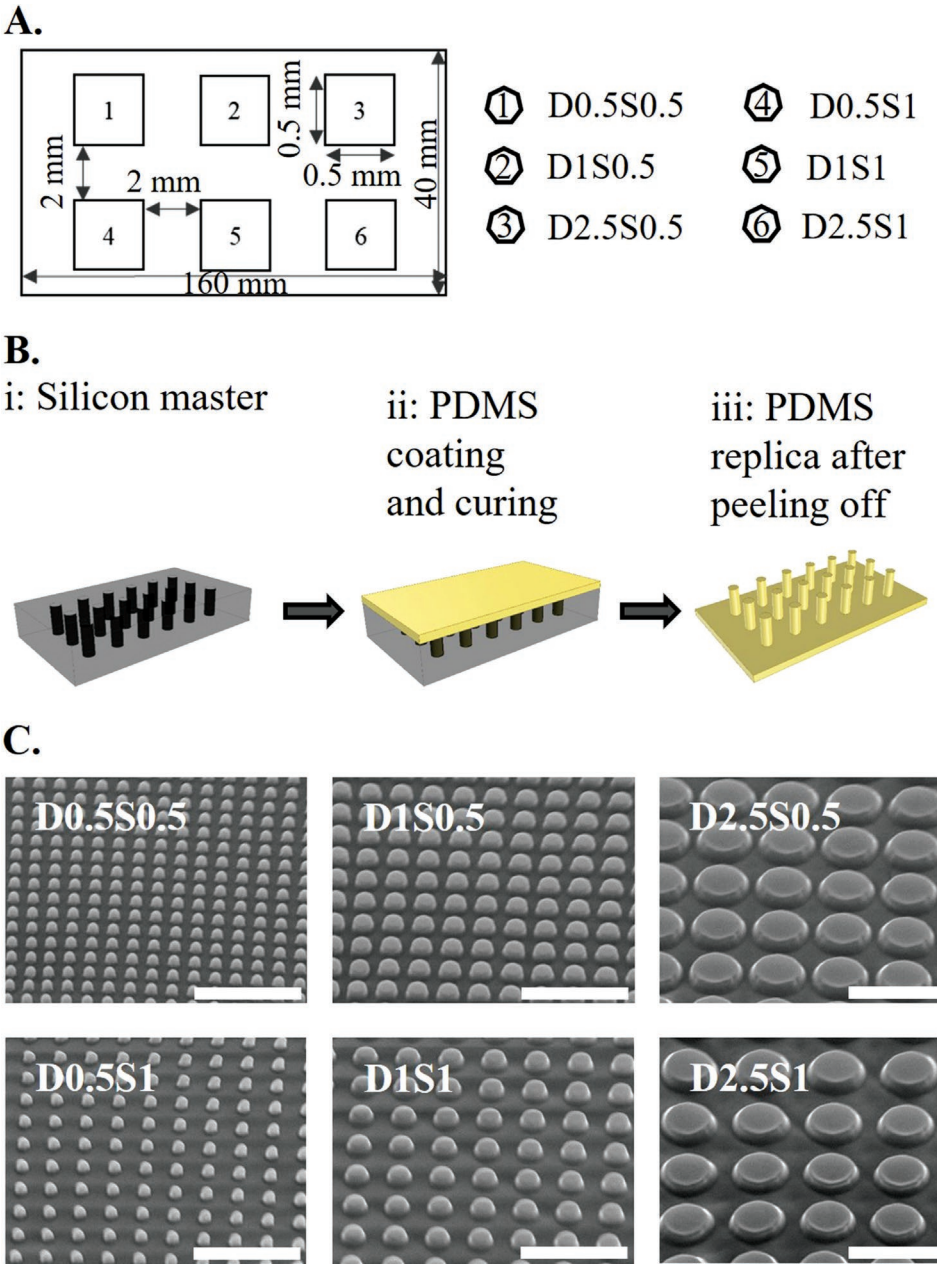

Figure 4. A) Schematic of the test specimen (the dimensions are not to scale). B) Fabrication of PDMS pillars, i) the silicon master mold with holes, ii) the mold is coated with PDMS and PDMS is cured, and iii) the cured PDMS is peeled off. C) SEM micrographs of the pillars with diameters ranging from 0.5 to 2.5 µm and spacing of 0.5 and 1 µm. Scale bars = 5 µm. The patterned surfaces are named with their diameter and spacing. For instance, D0.5S1 corresponds to the pillars with a diameter and spacing of 0.5 and 1 µm, respectively.

to be through the availability of a larger surface area for bacterial interactions compared to planar surfaces. In the case of smaller features (such as D0.5S0.5), due to the smaller spacings between the pillars, bacteria are mainly lodged on top of them (Figure S2A, Supporting Information).

Considering now the response of *E. coli* to the plasma-activated micro/nanopillars (**Figure 6** and Figure S2B, Supporting Information), the plasma treatment had a much greater effect on inhibiting bacterial adhesion when applied to structured surfaces. As emerged from the bacterial adhesion studies on planar surfaces, charge, and wettability both play key roles in inhibiting adhesion on plasma-activated surfaces. The wettability of the patterned area has not been investigated due to their small area (500 × 500 µm^2, Figure 4A), which restricts their contact angle measurements. However, it has been shown that the hydrophilicity of the plasma-treated surface is enhanced by plasma treatment, and the Wenzel model predicts that the wettability can be further enhanced by increasing the roughness.[78] Therefore, it is anticipated that the presence of the micro/nano features (which influence the surface roughness) results in a higher level of hydrophilicity on the plasma-treated structured samples compared to planar ones. Due to the

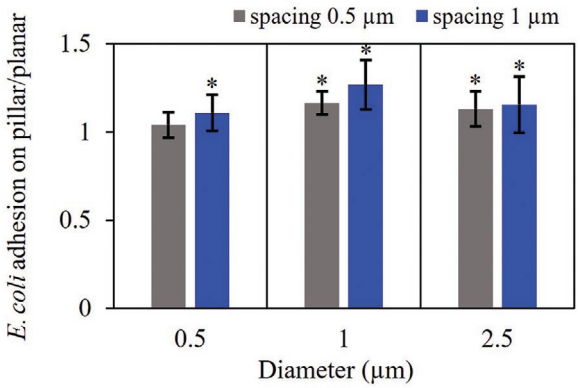

Figure 5. Ratio of *E. coli* adhesion on the native pillar (with different diameters and gap sizes) to native planar samples. * Represent that the adhesion on the pillar is significantly different from the planar control area ($n = 60$, $p < 0.05$). The error bar represents SD from three independent experiments.

high surface-to-volume area on the patterned features, a higher charge density is also expected of them. While the small area of the patterns hampers their direct measurement, the bacterial adhesion results from plasma-activated micro/nanopillars provide indirect, although compelling, evidence that surface charge and wettability were altered to a larger extent in structured surfaces. This can potentially be explained by the increased amount of silanol groups at the interface due to the larger surface area exposed for plasma activation, leading to higher hydrophilicity and surface charge density.[78] This behavior is consistent with the largest effect being observed for the 2 min aged surfaces, wherein the highest charge density and hydrophilicity existed.

Within the 2 min aged samples, plasma-treated nanopillars with the smallest dimensions (D0.5S0.5) showed the highest effect on preventing bacterial adhesion, with a reduction in the adhesion of 77.5% when compared with plasma-activated planar counterparts (**Figure 7**A). The lower adhesion can be potentially explained by the higher electrostatic repulsion force on the bacteria due to the high surface area for D0.5S0.5 (Figure 7C). These differences are even more apparent when one compares native structured surfaces with planar counterparts, where the opposite behavior was observed with higher bacterial adhesion for the structured surfaces (Figure S2A, Supporting Information).

The patterned surfaces with a gap size of 0.5 μm had less adhesion than those with a 1 μm gap. Inspection of fluorescence micrographs (Figure S2B, Supporting Information) reveals that bacteria adhered to patterned surfaces with a gap size of 1 μm mainly in the gaps between pillars, whereas adhesion was mainly on top of pillars on surfaces with a gap of 0.5 μm, presumably as the bacteria could not fit into the smaller gaps. Visual inspection did not reveal any major differences between the morphology of bacteria that attached to planar and structured surfaces (Figure S2, Supporting Information).

Equally interesting was the ability of the structured PDMS surfaces to sustain their antifouling properties for longer periods of storage than the planar PDMS, with the pillars of smaller diameter not reaching the values observed for planar counterparts after 50 days (Figure 7B). The bacterial coverage for D0.5S0.5, aged 2 min and 50 days is reduced by 98.7% and 65.1% compared to native planar control (Figure S4, Supporting Information). These results suggest that the smaller pillars (diameter of 0.5 μm) were capable of significantly delaying the hydrophobicity recovery, and this can potentially be explained

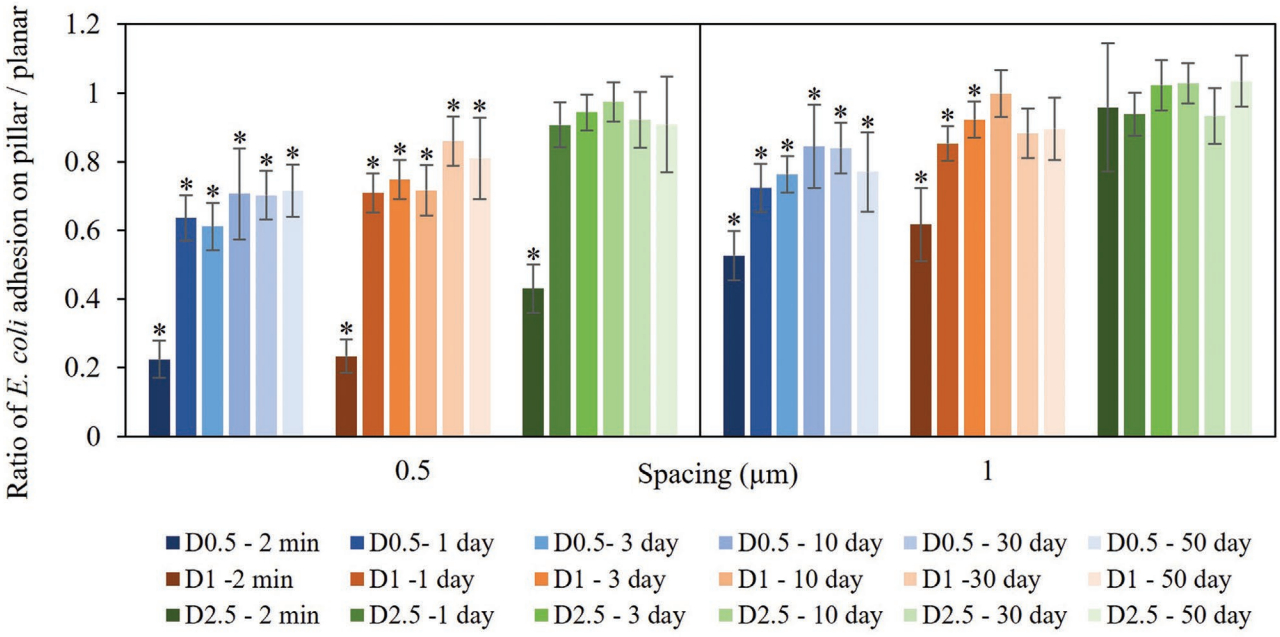

Figure 6. The ratio of *E. coli* adhesion on plasma-treated micro/nanopillars over plasma-treated planar control PDMS. The data labels represent the pillars' diameter and the age of the sample after plasma treatment. * Represent that the coverage on the pillar is significantly different from the planar area ($n = 60$, $p < 0.05$). The error bar represents SD from three independent experiments.

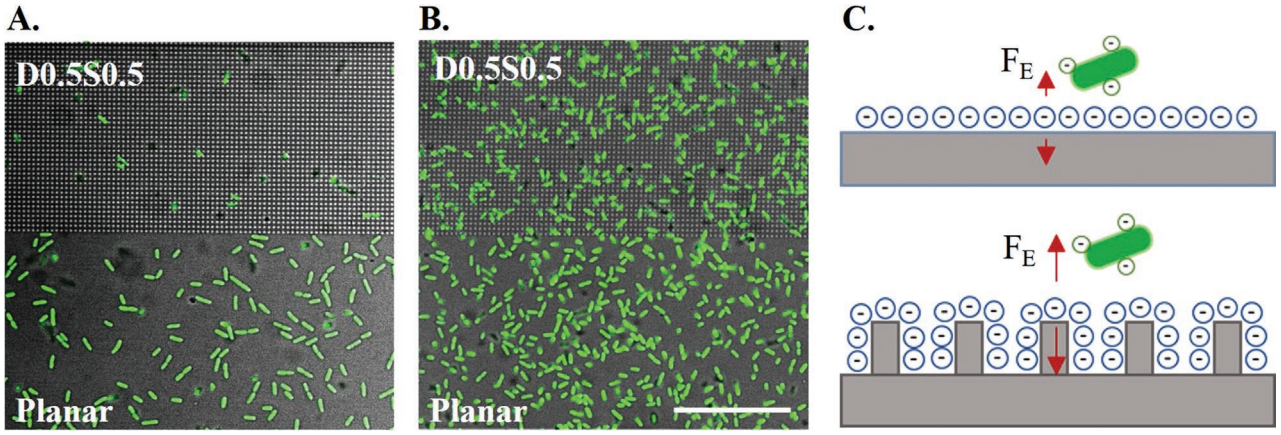

Figure 7. Comparison of *E. coli* adhesion between plasma-treated D0.5S0.5 and planar surfaces for A) 2 min and B) 50-day aged samples. Scale bars: 25 µm. C) Schematic effect of presence of nano topography on surface charge density and electrostatic interaction (F_E) between the bacteria and the surface.

by the constrained migration of free oligomers through the oxidized PDMS pillars.[79]

Figure 8 represents the percentage reduction in *E. coli* adhesion for plasma-treated patterned surfaces and the calculated surface area of each over a 500 × 500 µm planar area. The relationship between adhesion and surface area was shown to be dependent on the pillar spacing and diameter. While the percentage of reduction of adhesion decreases proportionally with a decrease in surface area for 0.5 µm spaces between pillars, no trend was observed between the surface area and the bacterial adhesion for the pillars with the spacing of 1 µm. For the latter, bacterial adhesion was promoted by increasing the diameter of the structured PDMS. A spacing of 1 µm had higher adhesion than 0.5 µm, presumably due to bacteria being able to adhere to the 1 µm but not the 0.5 µm spaces between pillars (Figure S2B, Supporting Information). The bacterial adhesion for D2.5 samples for all the aged groups, apart from 2 min aged samples, was similar to the planar area as their larger diameter allowed the bacteria to attach on top of them. The results suggest that D2.5 structures have undergone faster hydrophobic recovery than the other structures.

A time-lapse study has been performed to compare the adhesion of the bacteria over 2 h on 2 min aged plasma-treated D0.5S0.5 and the planar control sample. The sample was suspended with *E. coli* at $OD_{600} = 0.5$ for 30 min to provide enough time for the initial adhesion of the bacteria. Following that, the suspension was diluted 20 times with the fresh M63 medium to dissipate the planktonic cells. The adhesion of *E. coli* on an area with the boundaries of the pillar and the planar surface was monitored by capturing images every 2 min for 2 h (**Figure 9** and Video S1, Supporting Information). *E. coli* adhesion on the planar surface increased steadily over time, however, it was

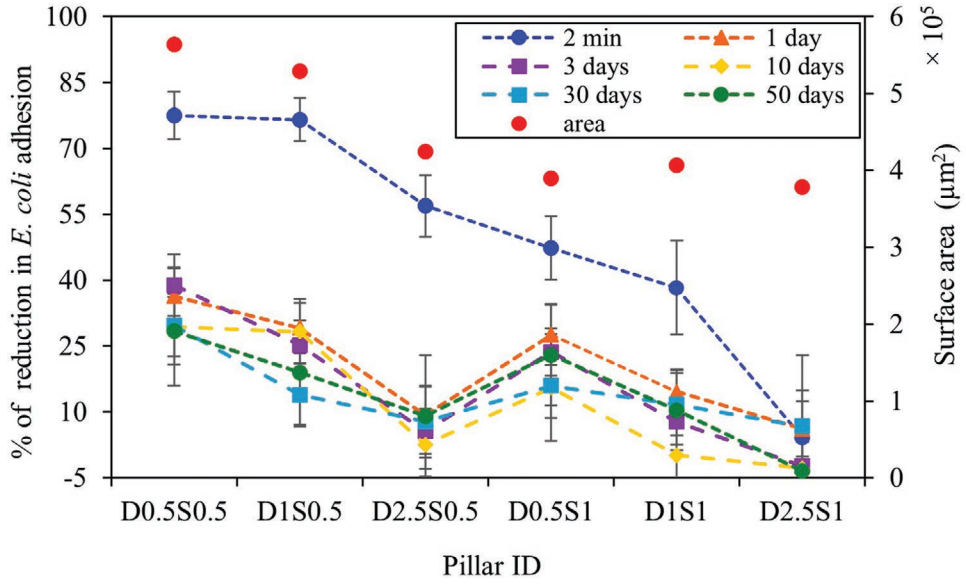

Figure 8. Percentage (%) of reduction in *E. coli* adhesion on aged plasma-treated pillars compared to its planar counterpart. Red dots represent the calculated surface area over the 500 × 500 µm² array for each feature size. The lines are only presented as an eye guide.

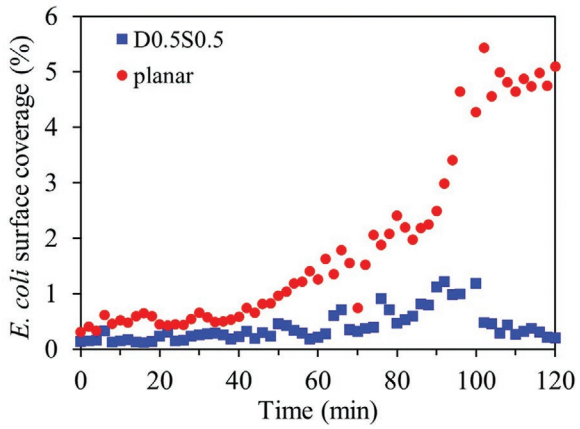

Figure 9. Time-lapse study of *E. coli* adhesion on plasma-treated D0.5S0.5 and planar over 2 h (Video S1, Supporting Information).

approximately constant for D0.5S0.5. Two factors appear to contribute to this observation: first, there were far fewer bacteria attached to the nanopillar surface than the planar; and second, bacteria attached to the planar surface were observed dividing whereas those attached to the nanopillars were not. Therefore, the nanopillars could be inhibiting both attachment and division of attached bacteria, similar to the drop in viability previously observed in other studies.[29]

The hydrophobic recovery of PDMS is mainly attributed to the migration of free oligomers from the bulk to the surface and possibly the reorientation of the polar species into the bulk.[80] To rationalize the reduced bacterial adhesion associated with slower recovery rates of hydrophobicity for the smaller nanopillar structures (D0.5S0.5), we propose that the mechanism is related to the geometric nanoconfinement effects. The reduction of structure size to the nanometer range has been shown to affect polymer molecular mobility,[81] and our results strongly suggest that similar nanoconfinement effects were exerted on the oligomer chains within the nanopillars. The physicochemical properties (charge density and hydrophilicity) of the plasma-activated surfaces were enhanced by confinement, and that enhancement depended on the size of the confined pillar interface and the confined space between the pillars. The smaller the interface and space, the larger the enhancement, leading to stronger anti-biofouling effects for the smaller pillars such as D0.5S0.5.

3. Conclusion

The results presented in this study revealed that the plasma treatment provokes a significant reduction in bacterial adhesion on structured surfaces relative to the planar control PDMS samples, and the effect remains there even after the aging of the PDMS samples. It has been shown that bacterial adhesion is affected by the dimension of the topological features and the surface hydrophobicity/hydrophilicity and charge. The findings of this study highlight the presence of the nanoconfinement effect for plasma-treated nanopillars which can serve as an effective strategy to enhance the anti-biofouling properties for nano topological features. Plasma-treated PDMS nanopillars with a diameter and spacing of 500 nm possess the highest antifouling properties against *E. coli*. In contrast, the antifouling efficiency reduces by increasing the pillar size to almost the level of control samples for pillars with a diameter of 2.5 µm. The presence of the submicron pillars and thus reduced contact area coupled with long-lasting increased hydrophilicity of the surface by plasma treatment are responsible for superior bacterial fouling resistance. The antifouling sustainability for the nanopillar structures is quite remarkable, with a 65.1% reduction compared to the native planar control sample after 50 days. Our study provides potential prospects to further enhance the antifouling properties of PDMS samples by the combination of the nanoconfinement effect and plasma treatment as a simple and cost-effective method.

4. Experimental Section

Fabrication of Master Mold and Preparation of PDMS Substrate: Micro/nano pattern holes were produced on a 4-inch single-side polished silicon wafer in Southampton Nanofabrication Centre, UK. The process involved e-beam lithography and patterning of the poly(methyl methacrylate) (PMMA) as a resist, followed by reactive ion etching (RIE) and removal of the PMMA.

PDMS substrates were fabricated using a silicone elastomer kit (Dow Corning Corporation, SYLGARD 184, USA) by mixing the base with the curing agent with a ratio of 10:1. The PDMS was mixed thoroughly using both components and degassed using a vacuum pump for 30 min to remove any trapped air bubble in the mixture. The mixture was then poured on a silicon wafer mold (plain or patterned with holes), degassed for another 30 min and cured at 40 °C for 48 h to fabricate 1 mm thick samples. The planar and patterned PDMS were cut into 1 × 1 and 1.6 × 0.5 cm^2 pieces, respectively. The side which was in direct contact with the silicon wafer was used to study bacteria and beads adhesion.

Plasma Treatment: The PDMS samples were placed in 35 mm polystyrene Petri dishes with triple vents, and air plasma-treated for 100 s using Harrick Plasma Cleaner PDC-32G-2 (Harrick Cleaner, New York, USA) at 18 W. Following the oxidization, sample dishes were covered with their lids and stored at 20 °C without extra sealing.

Contact Angle Measurements: Dynamic contact angle measurement was performed using the Theta Lite instrument (KSV Ltd., Helsinki, Finland) to characterize and compare the hydrophobicity of PDMS plasma-treated and native samples. The advancing and receding contact angles on the surface were measured using 5 µl of deionized water at 15 °C using the sessile drop technique.[82] Young–Laplace equation[83] was used to determine the right- and left-hand side contact angle, and the average value was used for comparison between different samples. The contact angle for each storage condition was averaged along three samples and five measurements for individual ones.

Surface Charge Density Measurement: The surface charge density of the PDMS samples was determined using the colorimetric method by measuring the amount of bounded Toluidine Blue O (TBO, Sigma Aldrich, Co., USA) on the PDMS samples.[45,65] TBO ($C_{15}H_{16}N_3S^+$) is a cationic blue dye that can be bounded to ionic charges and shows a light absorption peak at 633 nm.[84]

Each PDMS sample was immersed in 5 ml of 0.5 mM aqueous TBO solution (pH was adjusted to 10 using Na_2CO_3/$NaHCO_3$ buffer) for 6 h at 30 °C. Following that, the samples were washed using NaOH and each was placed in 50% (v/v) acetic acid for 24 h to obtain complete decomplexation of TBO from the sample surfaces; at this step the TBO molecules diffuse into the solution, coloring it blue. The latter solution was analyzed using the Evolution 300 UV–vis spectrophotometer (Thermo Scientific, UK) with an absorption peak at 633 nm. The measurements were performed in triplicate. The calibration curve

was obtained by measuring the optical density of TBO at a varying concentration in 50% acetic acid and was used to find the concentration of TBO on the surface of the PDMS samples. The control samples consisted of 50% acetic acid in contact with the untreated PDMS samples.

Due to the area of the patterned PDMS (0.5×0.5 cm^2), contact angle and surface charge measurements were only performed for the planar PDMS.

Microbial Culture and Micro Beads Preparation: *E. coli* K-12 SCC1 (MG1655 $P_{A1/04/03\text{-}gfpmut3*}$), which expresses green fluorescent protein (GFP),[69] was used for microbial culture. *E. coli* cells were taken from the frozen glycerol stocks and grown for 24 h on a nutrient agar plate at 37 °C. A single *E. coli* colony was inoculated in a 10 ml standard M63 minimal medium (contained 100 mM KH_2PO_4, 1 mM $MgSO_4$, 15 mM $(NH_4)_2SO_4$, 17 mM sodium succinate, 10 mM D-glucose and 1.8 µM $FeSO_4$) and allowed to grow in a shaking incubator (150 rpm) for 24 h at 30 °C. The cells were harvested by centrifugation at 3900 rpm for 5 min, the bacterial pellet was then resuspended in a fresh M63 medium to a final optical density of 0.5 at OD_{600}. 5 ml of the bacterial suspension was then added into the petri dish with the PDMS sample and incubated in a stationary incubator at 30 °C for 2 h. The experiments were conducted in triplicate for statistical analysis.

Fluorescent carboxylate-modified polystyrene (PS) beads with an average diameter of 1 µm (L4655, Sigma-Aldrich, Co., UK) were suspended in M63 minimal medium to the final optical density of 0.65 at OD600. 5 ml of the solution was added to the petri dish with the PDMS sample and incubated in a stationary incubator at 30 °C for 2 h.

Imaging: *E. coli* adhesion on PDMS samples was quantified on a standard fluorescent microscopy Axio Lab (Zeiss, Germany) with a 60x water objective equipped with a digital camera Motic image plus 3.0, or a Confocal Scanning Light Microscopy Leica TCS SP8 (Leica, Wetzlar, Germany) with a 40x water dipping objective lens and 2.5x digital zoom. For each sample, 20 images were collected randomly on the surface. Three biologically different replicas were examined for statistical analysis.

Hitachi TM3030 SEM was used to image the patterned PDMS. The samples were coated with 30 nm of platinum prior to the imaging and imaged using an accelerating voltage of 15 kV.

Image and Statistical Analysis: The percentage of the area coverage of *E. coli* and PS-COOH beads on the PDMS surfaces was quantified using ImageJ through an automated custom script to determine the fraction of area covered by cells in each picture.[85] The data collected (sample size $n = 60$) were statistically analyzed using ANOVA and Bonferroni post-hoc test. The presented data are reported as the mean ± SD. The data was considered statistically significant for $p < 0.05$. All statistical analysis was performed using MATLAB.

Supporting Information

Supporting Information is available from the Wiley Online Library or from the author.

Acknowledgements

D.B. was funded by the Biotechnology and Biological Sciences Research Council (BBSRC; http://www.bbsrc.ac.uk) grant number BB/J014532/1, through the Midlands Integrative Biosciences Training Partnership (MIBTP). The authors acknowledge financial support of this work by the EPSRC (EP/K027263/1) and ERC (Consolidator Grant 614787). The authors would like to acknowledge the Imaging Suite at the University of Birmingham for support of imaging experiments.

Conflict of Interest

The authors declare no conflict of interest.

Data Availability Statement

The data that support the findings of this study are available in the supplementary material of this article.

Keywords

antifouling, nano-pillar surface, plasma treatment, polydimethylsiloxane

Received: September 20, 2022
Revised: November 21, 2022
Published online:

[1] X. Khoo, M. W. Grinstaff, *MRS Bull.* **2011**, *36*, 357.
[2] J. G. Bartlett, *Infect. Dis. Clin. Pract.* **2004**, *12*, 258.
[3] V. B. Damodaran, N. S. Murthy, *Biomater. Res.* **2016**, *20*, 18.
[4] M. V. Graham, A. P. Mosier, T. R. Kiehl, A. E. Kaloyeros, N. C. Cady, *Soft Matter* **2013**, *9*, 6235.
[5] A. Terada, K. Okuyama, M. Nishikawa, S. Tsuneda, M. Hosomi, *Biotechnol. Bioeng.* **2012**, *109*, 1745.
[6] Y. J. Oh, E. S. Khan, A. n. d. Campo, P. Hinterdorfer, B. Li, *ACS Appl. Mater. Interfaces* **2019**, *11*, 29312.
[7] S. L. Arias, J. Devorkin, A. Civantos, J. P. Allain, *Langmuir* **2020**, *37*, 16.
[8] L. Cai, D. Wu, J. Xia, H. Shi, H. Kim, *Sci. Total Environ.* **2019**, *671*, 1101.
[9] J. B. Xavier, W. Kim, K. R. Foster, *Mol. Microbiol.* **2011**, *79*, 166.
[10] N. G. Kamatkar, J. D. Shrout, *PLoS One* **2011**, *6*, 20888.
[11] S. Wu, S. Altenried, A. Zogg, F. Zuber, K. Maniura-Weber, Q. Ren, *ACS Omega* **2018**, *3*, 6456.
[12] T. Wassmann, S. Kreis, M. Behr, R. Buergers, *Int. J. Implant Dent.* **2017**, *3*, 32.
[13] X. Ge, Y. Leng, X. Lu, F. Ren, K. Wang, Y. Ding, M. Yang, *J. Biomed. Mater. Res., Part A* **2015**, *103*, 384.
[14] W. Choi, E. P. Chan, J.-H. Park, W.-G. Ahn, H. W. Jung, S. Hong, J. S. Lee, J.-Y. Han, S. Park, D.-H. Ko, *ACS Appl. Mater. Interfaces* **2016**, *8*, 31433.
[15] M. Katsikogianni, Y. Missirlis, *Acta Biomater.* **2010**, *6*, 1107.
[16] S. Zheng, M. Bawazir, A. Dhall, H.-E. Kim, L. He, J. Heo, G. Hwang, *Front. Bioeng. Biotechnol.* **2021**, *9*, 82.
[17] J. Ye, J. Deng, Y. Chen, T. Yang, Y. Zhu, C. Wu, T. Wu, J. Jia, X. Cheng, X. Wang, *Biomater. Sci.* **2019**, *7*, 2826.
[18] H. Shahali, J. Hasan, A. Mathews, H. Wang, C. Yan, T. Tesfamichael, P. K. Yarlagadda, *J. Mater. Chem. B* **2019**, *7*, 1300.
[19] E. P. Ivanova, J. Hasan, H. K. Webb, G. Gervinskas, S. Juodkazis, V. K. Truong, A. H. Wu, R. N. Lamb, V. A. Baulin, G. S. Watson, *Nat. Commun.* **2013**, *4*, 2838.
[20] F. Dundar Arisoy, K. W. Kolewe, B. Homyak, I. S. Kurtz, J. D. Schiffman, J. J. Watkins, *ACS Appl. Mater. Interfaces* **2018**, *10*, 20055.
[21] H.-W. Chien, X.-Y. Chen, W.-P. Tsai, M. Lee, *Colloids Surf., B* **2020**, *186*, 110738.
[22] C. M. Bhadra, V. K. Truong, V. T. Pham, M. Al Kobaisi, G. Seniutinas, J. Y. Wang, S. Juodkazis, R. J. Crawford, E. P. Ivanova, *Sci. Rep.* **2015**, *5*, 16817.
[23] H. J. Ensikat, P. Ditsche-Kuru, C. Neinhuis, W. Barthlott, *Beilstein J. Nanotechnol.* **2011**, *2*, 152.
[24] B. Dean, B. Bhushan, *Philos. Trans. R. Soc., A* **2010**, *368*, 4775.
[25] S. M. Kelleher, O. Habimana, J. Lawler, B. O'reilly, S. Daniels, E. Casey, A. Cowley, *ACS Appl. Mater. Interfaces* **2016**, *8*, 14966.
[26] E. P. Ivanova, J. Hasan, H. K. Webb, V. K. Truong, G. S. Watson, J. A. Watson, V. A. Baulin, S. Pogodin, J. Y. Wang, M. J. Tobin, *Small* **2012**, *8*, 2489.

[27] G. S. Watson, D. W. Green, L. Schwarzkopf, X. Li, B. W. Cribb, S. Myhra, J. A. Watson, *Acta Biomater.* **2015**, *21*, 109.
[28] D. E. Mainwaring, S. H. Nguyen, H. Webb, T. Jakubov, M. Tobin, R. N. Lamb, A. H.-F. Wu, R. Marchant, R. J. Crawford, E. P. Ivanova, *Nanoscale* **2016**, *8*, 6527.
[29] J. Hasan, S. Raj, L. Yadav, K. Chatterjee, *RSC Adv.* **2015**, *5*, 44953.
[30] T. Diu, N. Faruqui, T. Sjöström, B. Lamarre, H. F. Jenkinson, B. Su, M. G. Ryadnov, *Sci. Rep.* **2014**, *4*, 7122.
[31] L. Mi, S. Jiang, *Angew. Chem., Int. Ed.* **2014**, *53*, 1746.
[32] S. W. Lee, K. S. Phillips, H. Gu, M. Kazemzadeh-Narbat, D. Ren, *Biomaterials* **2021**, *268*, 120595.
[33] G. C. Ling, M. H. Low, M. Erken, S. Longford, S. Nielsen, A. J. Poole, P. Steinberg, D. McDougald, S. Kjelleberg, *Biofouling* **2014**, *30*, 323.
[34] P. Halder, M. Nasabi, N. Jayasuriya, J. Shimeta, M. Deighton, S. Bhattacharya, A. Mitchell, M. A. Bhuiyan, *Biofouling* **2014**, *30*, 695.
[35] F. Song, D. Ren, *Langmuir* **2014**, *30*, 10354.
[36] T. S. Heckmann, J. D. Schiffman, A. C. S. Appl, *Nano Mater.* **2019**, *3*, 977.
[37] P. Papadopoulos, B.-E. Pinchasik, M. Tress, D. Vollmer, M. Kappl, H.-J. Butt, *Soft Matter* **2018**, *14*, 7429.
[38] D. Perera-Costa, J. M. Bruque, M. a. L. González-Martín, A. C. Gómez-García, V. Vadillo-Rodriguez, *Langmuir* **2014**, *30*, 4633.
[39] N. Lu, W. Zhang, Y. Weng, X. Chen, Y. Cheng, P. Zhou, *Food Control* **2016**, *68*, 344.
[40] R. S. Friedlander, H. Vlamakis, P. Kim, M. Khan, R. Kolter, J. Aizenberg, *Proc. Natl. Acad. Sci. U. S. A.* **2013**, *110*, 5624.
[41] M. J. Owen, P. J. Smith, *J. Adhes. Sci. Technol.* **1994**, *8*, 1063.
[42] D. Bodas, C. Khan-Malek, *Sens. Actuators, B* **2007**, *123*, 368.
[43] A. Reisner, M. Maierl, M. Jörger, R. Krause, D. Berger, A. Haid, D. Tesic, E. L. Zechner, *J. Bacteriol.* **2014**, *196*, 931.
[44] L. Crémet, S. Corvec, P. Bémer, L. Bret, C. Lebrun, B. Lesimple, A.-F. Miegeville, A. Reynaud, D. Lepelletier, N. Caroff, *J. Infect.* **2012**, *64*, 169.
[45] O. Rzhepishevska, S. Hakobyan, R. Ruhal, J. Gautrot, D. Barbero, M. Ramstedt, *Biomater. Sci.* **2013**, *1*, 589.
[46] V. Jokinen, P. Suvanto, S. Franssila, *Biomicrofluidics* **2012**, *6*, 016501.
[47] H. Hillborg, J. Ankner, U. W. Gedde, G. Smith, H. Yasuda, K. Wikström, *Polymer* **2000**, *41*, 6851.
[48] A. Mata, A. J. Fleischman, S. Roy, *Biomed. Microdevices* **2005**, *7*, 281.
[49] M. Amerian, M. Amerian, M. Sameti, E. Seyedjafari, *J. Biomed. Mater. Res., Part A* **2019**, *107*, 2806.
[50] C. de Menezes Atayde, I. Doi, *Phys. Status Solidi C* **2010**, *7*, 189.
[51] M. Morra, E. Occhiello, R. Marola, F. Garbassi, P. Humphrey, D. Johnson, *J. Colloid Interface Sci.* **1990**, *137*, 11.
[52] B. T. Ginn, O. Steinbock, *Langmuir* **2003**, *19*, 8117.
[53] R. A. Lawton, C. R. Price, A. F. Runge, W. J. DohertyIII, S. S. Saavedra, *Colloids Surf. A* **2005**, *253*, 213.
[54] I.-J. Chen, E. Lindner, *Langmuir* **2007**, *23*, 3118.
[55] Y.-W. Cheng, C.-W. Hsiao, Z.-L. Zeng, W.-L. Syu, T.-Y. Liu, *Surf. Coat. Technol.* **2020**, *389*, 125653.
[56] F. Jahangiri, T. Hakala, V. Jokinen, *Microfluid. Nanofluid.* **2020**, *24*, 2.
[57] H. Hillborg, U. Gedde, *Polymer* **1998**, *39*, 1991.
[58] E. P. Everaert, H. C. Van Der Mei, H. J. Busscher, *J. Adhes. Sci. Technol.* **1996**, *10*, 351.
[59] I. Hoek, F. Tho, W. M. Arnold, *Lab Chip* **2010**, *10*, 2283.
[60] J. Bacharouche, H. Haidara, P. Kunemann, M.-F. Vallat, V. Roucoules, *Sens. Actuators, A* **2013**, *197*, 25.
[61] X. Ren, M. Bachman, C. Sims, G. Li, N. Allbritton, *J. Chromatogr. B: Biomed. Sci. Appl.* **2001**, *762*, 117.
[62] W. K. T. Coltro, S. M. Lunte, E. Carrilho, *Electrophoresis* **2008**, *29*, 4928.
[63] V. Tandon, S. K. Bhagavatula, W. C. Nelson, B. J. Kirby, *Electrophoresis* **2008**, *29*, 1092.
[64] E. Uchida, Y. Uyama, Y. Ikada, *Langmuir* **1993**, *9*, 1121.
[65] M. Ciobanu, A. Siove, V. Gueguen, L. Gamble, D. Castner, V. Migonney, *Biomacromolecules* **2006**, *7*, 755.
[66] B. J. Kirby, E. F. Hasselbrinkjr, *Electrophoresis* **2004**, *25*, 203.
[67] Z. Liu, Y. Song, D. Li, *J. Colloid Interface Sci.* **2020**, *578*, 116.
[68] B. Wang, Z. Abdulali-Kanji, E. Dodwell, J. H. Horton, R. D. Oleschuk, *Electrophoresis* **2003**, *24*, 1442.
[69] H. Miao, S. Ratnasingam, C. San Pu, M. M. Desai, C. C. Sze, *J. Microbiol. Methods* **2009**, *76*, 109.
[70] C. Gómez-Suárez, H. J. Busscher, H. C. van der Mei, *Appl. Environ. Microbiol.* **2001**, *67*, 2531.
[71] D. Wang, Y. Fu, J. Yan, B. Zhao, B. Dai, J. Chao, H. Liu, D. He, Y. Zhang, C. Fan, S. Song, *Anal. Chem.* **2014**, *86*, 1932.
[72] K. A. Soni, A. K. Balasubramanian, A. Beskok, S. D. Pillai, *Curr. Microbiol.* **2008**, *56*, 93.
[73] H. Straub, C. M. Bigger, J. Valentin, D. Abt, X. H. Qin, L. Eberl, K. Maniura-Weber, Q. Ren, *Adv. Healthcare Mater.* **2019**, *8*, 1801323.
[74] R. Helbig, D. Günther, J. Friedrichs, F. Rößler, A. Lasagni, C. Werner, *Biomater. Sci.* **2016**, *4*, 1074.
[75] M. S. Gangan, C. A. Athale, *R. Soc. Open Sci.* **2017**, *4*, 160417.
[76] K. A. Whitehead, J. Verran, *Food Bioprod. Process.* **2006**, *84*, 253.
[77] Q. Li, Z. Xu, I. Pinnau, *J. Membr. Sci* **2007**, *290*, 173.
[78] R. N. Wenzel, *Ind. Eng. Chem.* **1936**, *28*, 988.
[79] T. Tsuzuki, K. Baassiri, Z. Mahmoudi, A. S. Perumal, K. Rajendran, G. M. Rubies, D. V. Nicolau, *Materials* **2022**, *15*, 2313.
[80] H. Hillborg, M. Sandelin, U. W. Gedde, *Polymer* **2001**, *42*, 7349.
[81] R. Winkler, A. Beena Unni, W. Tu, K. Chat, K. Adrjanowicz, *J. Phys. Chem. B* **2021**, *125*, 5991.
[82] S. Srinivasan, G. H. McKinley, R. E. Cohen, *Langmuir* **2011**, *27*, 13582.
[83] Y. Yuan, T. R. Lee, S. Ser, *Surf. Sci.* **2013**, *51*, 3.
[84] B. Saha, S. Chowdhury, D. Sanyal, K. Chattopadhyay, G. S. Kumar, *ACS Omega* **2018**, *3*, 2588.
[85] M. D. Abràmoff, P. J. Magalhães, S. J. Ram, *Biophotonics Int.* **2004**, *11*, 36.